

High harmonic generation from bulk diamond driven by intense femtosecond laser pulse

Tzveta Apostolova, Boyan Obreshkov

Institute for Nuclear Research and Nuclear Energy,

Bulgarian Academy of Sciences, Tsarigradsko chaussee 72, Sofia 1784, Bulgaria

We present theoretical results on the high-harmonic generation (HHG) in bulk diamond induced by intense laser pulse of wavelength 800 nm, having a time duration of 15 fs. For laser intensity in the range $I \in [1, 50]$ TW/cm², above bandgap harmonics are generated after the pulse peak. We find that the intensity of individual harmonic peaks increases non-linearly as the laser intensity increases. For moderate laser intensity, the HHG spectrum exhibits a primary plateau with noisy odd order harmonic structure and sharp cutoff. For increased laser intensity a secondary plateau emerges with quasi-continuous spectrum of harmonics extending beyond the 50th order. Consistently with experimental observations, we find that the cutoff energy for HHG scales linearly with the peak field strength and heuristic derivation of the cutoff law is provided.

I. INTRODUCTION

Diamond is a material, exhibiting unique mechanical, thermal and electronic properties, such as the high electron and hole mobilities and the high breakdown field strength¹. Ultrashort laser pulses and their application to laser-matter interaction have shown great progress during the last few decades. In particular, high-harmonic generation (HHG) is one of the most important phenomena in the strong-field laser-matter interaction. HHG is a secondary process of non-linear laser frequency conversion to its multiples driven by the strong coupling of the oscillating electric field of an intense ultrashort laser pulse to electrons. HHG has been investigated experimentally and theoretically over a broad range of laser intensities and wavelengths, in gaseous and molecular targets²⁻⁷, plasmas⁸ and in the solid state⁹. The experiments have shown that sources based on high harmonic generation (HHG) have spatial and temporal coherence, high directionality and polarization but due to the low efficiency of the process, the intensities of the generated harmonics are orders of magnitude lower than that of the exciting field hence less intense than EUV, XUV and soft x-ray radiation produced in the huge facilities such as FEL accelerator¹⁰ and Synchrotron Radiation (SR)¹¹. Nevertheless they can be potentially used to obtain coherent radiation of sub-femtosecond to attosecond duration in a broad wavelength range (XUV to X-ray)¹²⁻¹⁵ capable of inducing physical processes on very short time and space scales leading to applications such as attosecond electron dynamics¹⁶, molecular tomography and protein crystallography¹⁷, etc.

Generation of high harmonics in the gas phase is usually described by a semi-classical three step model¹⁸⁻²⁰, including field ionization, followed by the acceleration of the photoelectron and its subsequent recombination with the parent ion resulting in emission of single energetic photon. HHG spectra typically consist of sub-bandgap harmonics with rapidly decreasing intensity in agreement with perturbation theory, a plateau region of above bandgap harmonics with a high energy cutoff

where the harmonic intensity drops off abruptly. The cutoff energy of the gas-phase harmonics depends linearly on the laser intensity according to the famous relation $\hbar\omega_{\max} \approx I_p + 3.17U_p$, where I_p is the atomic ionization potential and U_p is the pondermotive energy.

Experimental studies of HHG in semiconductors and dielectrics have been reported recently, e.g.^{9,21,22}. In solid crystals the interplay between generation of carriers via multiphoton excitation over the bandgap at high intensities leading to catastrophic breakdown of the material and HHG is carefully explored to find regimes in which only HHG takes place avoiding material collapse. In the pioneering study of Ghimire et al.⁹ long wavelength laser radiation is used to suppress multiphoton ionization and to obtain HHG. Experimental and theoretical study of HHG spectra from rare-gas solids²¹ exposed characteristic features of HHG in solids: emergence of multiple plateaus as the driving laser intensity increases over a narrow intensity range that consists of a few harmonics; complicated dependence of the cutoff on the driving laser field, i.e. following neither linear nor square-root scaling; photon energy of the HHG in solids exceeding the maximum band separation between the highest-valence and lowest-conduction bands.

Various theoretical models have been proposed to rationalize HHG in crystalline solids including HHG in diamond varying from time-dependent-density-functional-theory,²³⁻²⁶ time-dependent-Schrodinger-equation (TDSE)^{27,28}, semiconductor Bloch equations^{29,30} and semiclassical methods³¹ the latter being more intuitive than the former. The underlying microscopic processes are still explored to elucidate further the dependence of HHG in solids on the electronic band structure and on the interplay between inter- and intraband transitions as well as on the collective behavior of the high density electron-hole plasma coupled to the lattice. In this respect methods based on the TDSE in single-particle approximation incorporating realistic band structure may provide helpful insight on the mechanisms of HHG in solids.

In view of the fact that HHG in wide band-gap semi-

conductors may lead to brighter sources due to the high laser induced carrier density and ability to withstand the driving laser fields necessary for inducing strong nonlinear and non perturbative effects leading to HHG in the present work we explore the feasibility for sub-femtosecond pulse generation in diamond bulk subjected to intense 15 fs laser pulse with mid-infrared wavelength. The paper is organized as follows: In Section II the theoretical framework of photoexcitation and generation of high harmonics is presented. Section III presents numerical results and discussion of HHG spectra.

II. THEORETICAL DESCRIPTION

We describe the electron dynamics in a unit cell of crystalline diamond subjected to spatially uniform laser electric field $\mathbf{F}(t)$ with the time-dependent Schrödinger equation in single-active electron approximation

$$i\partial_t|\psi_{v\mathbf{k}}(t)\rangle = H(t)|\psi_{v\mathbf{k}}(t)\rangle, \quad (1)$$

where $v\mathbf{k}$ labels the initially occupied valence band states of definite crystal momentum \mathbf{k} and

$$H(t) = \frac{1}{2}[\mathbf{p} + \mathbf{A}(t)]^2 + V(\mathbf{r}), \quad (2)$$

is the time-dependent Hamiltonian written in velocity gauge with $\mathbf{F}(t) = -\partial_t\mathbf{A}(t)$, $\mathbf{p} = -i\nabla_{\mathbf{r}}$ is the momentum operator, $V(\mathbf{r})$ is an empirical ion-lattice pseudopotential

$$V(\mathbf{r}) = \sum_{\mathbf{G}} V(G) \cos(\mathbf{G} \cdot \boldsymbol{\tau}) e^{i\mathbf{G} \cdot \mathbf{r}}, \quad (3)$$

here $2\boldsymbol{\tau} = a_0(1/4, 1/4, 1/4)$ is a relative vector connecting two carbon atoms in a crystal unit cell, $a_0 = 3.57 \text{ \AA}$ is the bulk lattice constant and \mathbf{G} labels the reciprocal lattice wave-vectors. In Eq.(3), the pseudopotential formfactors $V(G)$ (in Rydberg) are $V(G^2 = 3) = 0.625$, $V(G^2 = 8) = 0.051$, and $V(G^2 = 11) = 0.206$; here the wave number G is given in units of $2\pi/a_0$. The pseudpotential parameters reproduce the principal energy gaps of the static band structure of diamond, the indirect bandgap of 5.42 eV and direct gap of $\Delta = 7.08 \text{ eV}$ at the BZ center.

We solve numerically Eq.(1) using a basis set expansion over static Bloch orbitals³². The bulk band structure is represented by the 4 valence bands and $N_c = 16$ unoccupied conduction bands. The Brillouin zone (BZ) was sampled by a Monte Carlo method using 3000 randomly generated \mathbf{k} -points. The laser vector potential was assumed to be a temporally Gaussian pulse $\mathbf{A}(t) = (F/\omega_L)\mathbf{e} \exp(-\ln(4)t^2/\tau^2) \sin \omega_L t$, where $\hbar\omega_L = 1.55 \text{ eV}$ is the photon energy, $\tau = 15 \text{ fs}$ is the time duration and \mathbf{e} is a unit vector in the direction of laser polarization; the crystal was irradiated by a single pulse linearly polarized along the Λ line (Γ -L direction). The time-step for the numerical integration of the equation of motion was $\delta t = 0.03 \text{ a.u.}$

The optically-induced electron current in the direction of the laser electric field \mathbf{e} is given by the BZ integral

$$J(t) = \int_{\text{BZ}} \frac{d^3\mathbf{k}}{4\pi^3} J(\mathbf{k}, t) \quad (4)$$

where

$$J(\mathbf{k}, t) = \sum_v \langle \psi_{v\mathbf{k}}(t) | \mathbf{e} \cdot \mathbf{v}(t) | \psi_{v\mathbf{k}}(t) \rangle, \quad (5)$$

and $\mathbf{v}(t) = \mathbf{p} + \mathbf{A}(t)$ is the velocity operator. The HHG spectrum can be presented as a coherent sum

$$I(\omega) = \left| \int_{\text{BZ}} \frac{d^3\mathbf{k}}{4\pi^3} J_{\mathbf{k},\omega} \right| \quad (6)$$

over contributions from Bloch states with wave-vector \mathbf{k}

$$J_{\mathbf{k},\omega} = \int dt e^{i\omega t} J(\mathbf{k}, t). \quad (7)$$

III. NUMERICAL RESULTS AND DISCUSSION OF HIGH HARMONIC SPECTRA

In Fig.1(a-c) we plot the time evolution of the velocity distribution of electrons for peak laser intensities $I = 2, 10$ and 30 TW/cm^2 , respectively. In the low-intensity regime, Fig.1(a), the distribution follows quasi-adiabatically the laser vector potential with

$$J(\mathbf{k}, t) \approx J^{\text{ad}}(\mathbf{k}, t) = \sum_v \mathbf{e} \cdot \nabla_{\mathbf{k}} \varepsilon_v(\mathbf{k}) \Big|_{\mathbf{k}=\mathbf{k}(t)} \quad (8)$$

where $\mathbf{k}(t) = \mathbf{k} + \mathbf{A}(t)$ is the shifted crystal momentum and $\varepsilon_v(\mathbf{k})$ are dispersion curves for valence electrons. For the increased intensity with $I = 10 \text{ TW/cm}^2$, Fig.1(b), the velocities near the BZ edges follow the adiabatic time evolution, however states near the BZ center do not have enough time to fully equilibrate against the laser vector potential, such that the velocity distribution is strongly distorted after the peak of the pulse. As a consequence the non-linear polarization current near the Γ point undergoes very rapid sub-cycle changes resulting in generation of high harmonics after the pulse peak. In the high-intensity regime with $I = 30 \text{ TW/cm}^2$, as shown in Fig.1(c), the velocity distribution is strongly distorted at the BZ center and this non-adiabatic distortion extends towards the BZ edges.

The optically induced currents are shown in Fig. 2(a-c) for the three different laser intensities discussed above. Stable and reversible (free from breakdown) ultrafast currents following the laser vector potential are induced, cf. Fig. 2(a-b). These AC currents are due to asymmetry of the velocity distribution of charge carriers in \mathbf{k} -space. For the increased laser intensity, the rapid current density oscillations exhibited in the wake of the pulse become prominent as a direct consequence of the build up of coherent superposition of populations in the valence and conduction bands.

The spectral line strength $I(\mathbf{k}, \omega) = |J_{\mathbf{k}\omega} + J_{-\mathbf{k},\omega}|$ for the Λ line is shown in Fig.3(a-c). For relatively weak and moderate peak laser intensity, Fig.3(a-b), the odd harmonic structure of the velocity distribution is clearly exhibited. For the lowest intensity shown in Fig.3(a), sub-bandgap harmonics extend from the BZ center towards the edges. The rapid sub-cycle distortion of the velocities near the BZ center gives rise to emission of intense 5th harmonic, the 7th order is highly virtual and suppressed. For the increased laser intensity with $I = 10$ TW/cm² shown in Fig.3(b), the HHG spectrum is characterized by a plateau region above the bandgap with cutoff at the position of the 9th harmonic. The lack of even order harmonics is because for monochromatic laser irradiation with $A(t) = (F/\omega_L) \sin \omega_L t$, the time-dependent Hamiltonian in Eq.(2) is invariant under the combined transformation of spatial inversion $\mathbf{r} \rightarrow -\mathbf{r}$ supplemented by time translation on half of the laser period $t \rightarrow t + \pi/\omega_L$. Because of this dynamical symmetry, the coefficients in the Fourier series in t : $J(\mathbf{k}, t) = \sum_n J_n(\mathbf{k}) \exp(in\omega_L t)$, satisfy the relation $J_n(\mathbf{k}) = -(-1)^n J_n(-\mathbf{k})$, so that all even order harmonics interfere destructively and do not contribute to the total HHG current. For the highest intensity shown in Fig.3(c), the spectrum extends to higher orders and the clear odd-harmonic structure is smeared out. The primary plateau extends to 15th order, decreases gradually in spectral intensity with the increase of the harmonic order and crosses over into a secondary plateau with harmonics extending above the 50th order.

Fig. 4(a-c) shows HHG spectra for the three peak laser intensities $I = 2, 10$ and 30 TW/cm². For the low intensity shown in Fig.4(a), HHG is characterized the 1st and 3rd sub-bandgap harmonics and the 5th bandgap harmonic. The HHG ends abruptly at the position of 5th harmonic, such that for relatively weak laser field the high-energy cutoff is determined by the direct bandgap. For the increased laser intensity shown in Fig.4(b), the spectrum extends to higher harmonic orders, the primary plateau emerges with cut-off at the position of 9th harmonic. The discrete character of individual harmonics above the bandgap is blurred. This lack of clear odd-harmonic structure can be rationalized within the semi-classical re-collision model as due interferences of multiple re-collisions between electron-hole pairs with different total energies at different times of recombination³¹. For the highest peak intensity $I = 30$ TW/cm² shown in Fig.4(c), HHG is characterized by a quasi-continuous spectrum of harmonics and emergence of weak secondary plateau with cutoff positioned at the 50th harmonic. This secondary plateau with harmonic orders extending beyond the atomic limit of the corresponding gas-phase harmonics suggests sensitive dependence of HHG on the band structure of diamond; Fig.5 demonstrates that when the total number of available conduction bands is reduced from $N_c = 16$ to 1, the secondary plateau is diminished, which makes evident that this plateau originates in the recombination of highly promoted conduction electrons with valence band holes. Similar results

are found in HHG spectra from rare-gas solids²¹.

In Fig.6 we plot the field dependence of the spectral intensity of individual harmonics S_n in the first plateau region. For the fixed pulse length, the laser intensity dependence can be divided into 3 regimes. I. Perturbative regime: The 3rd and the 5th harmonic are distinguishable and scaling law $S_n \sim F^n$ is exhibited. II. Intermediate regime (with $F \sim 1$ V/nm): The HHG spectrum extends to higher orders as the field strength increases. The intensity of different harmonic orders exhibit the power law $S_n \sim F^6$ regardless on the harmonic order. III. High field strength with $F \geq 5$ V/nm: the intensity of individual harmonics become indistinguishable.

Fig.7(a-b) shows the field-dependence of the photon-energy cutoff for the primary and secondary plateau, respectively. In contrast to the cutoff law observed for gas-phase harmonics, cutoff harmonics generated from diamond bulk display linear scaling with the field strength F . This linear scaling law is consistent with experimental observations in ZnO⁹. The high-energy cutoff of the secondary plateau can be distinguished for strong fields with $F \sim 0.4$ V/Å corresponding to laser intensity $I > 10$ TW/cm². The slope of this linear dependence implies that the cutoff energy increases by 2 harmonic orders when the field strength is increased by 0.5 V/nm. In contrast, the slope of the photon-energy cutoff of the primary plateau is flatter by a factor of 3. This linear scaling law is a consequence of the specific dispersion law between energy and momentum for Bloch electrons. For localized (in momentum space) excitation of electron-hole pairs near the Brillouin zone center with wave-vector $\mathbf{k} \approx \mathbf{0}$, the total energy of the charge carriers moving in the laser field can be written in relativistic form (cf. Ref.³³) with $\Delta(\mathbf{k}(t)) = \Delta \sqrt{1 + \mathbf{k}^2(t)/m\Delta}$, where $m \approx 0.07$ is the reduced mass of the pair. Within the classical re-collision model³¹, an electron-hole pair is born at rest near the peak of a laser field, the field accelerates away the carriers, which then recombine radiatively at a later time as the field reverses direction. The maximal energy gained at the time of recombination is $E_{\max} \approx \Delta \sqrt{1 + 1/\gamma_K^2}$, where $\gamma_K = \omega_L \sqrt{m\Delta}/F$ is the Keldysh parameter, so that for strong laser fields with $\gamma_K \ll 1$ (as in the present paper), we have $E_{\max} \approx \Delta/\gamma_K$ which heuristically explains the linear scaling law of the cutoff energy for HHG.

IV. CONCLUSION

In summary, we presented calculation of HHG spectrum from bulk diamond induced by an intense femtosecond laser pulse. Our result describes the intense HHG extending from the perturbative to highly non-perturbative incident laser intensity regimes. The non-perturbative regime of HHG occurs for laser intensity $I \geq 1$ TW/cm². We find that depending on the laser intensity, the HHG spectra from bulk diamond exhibits two plateau regions with above bandgap harmonics, the secondary plateau extends beyond the limit of the corresponding gas-phase

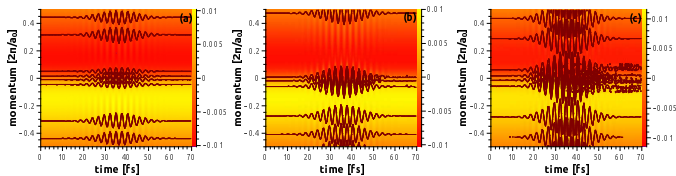


FIG. 1. Velocity distribution of electrons along the Λ -line in diamond bulk driven by intense laser pulse with wavelength 800 nm and time duration 15 fs. The peak laser intensity is: (a) $I=2$ TW/cm², (b) $I=10$ TW/cm² and (c) $I=30$ TW/cm²

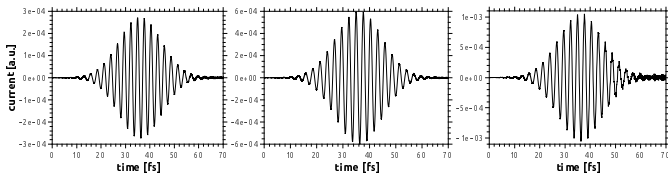


FIG. 2. Currents in diamond bulk driven by an intense laser pulse with wavelength 800 nm and time duration 15 fs. The peak laser intensity is: (a) $I=2$ TW/cm², (b) $I=10$ TW/cm² and (c) $I=30$ TW/cm²

harmonics emitted for the same laser intensity. The appearance of multiple plateaus turns out to be specific

for HHG in solids characterized by strong interband couplings between multiple single-particle states. The linear scaling law of cutoff energy for HHG is sensitive to the concrete type of energy-momentum dispersion law for Bloch electrons. The numerical results make evident the feasibility of diamond for sub-femtosecond pulse generation.

ACKNOWLEDGEMENTS

This work is supported by the Bulgarian National Science Fund under Contract No. DFNI-E02/6 and Contract No. DNTS/France-01/9 (T.A.) and by the Bulgarian National Science Fund under Contract No. 08-17 (B.O.).

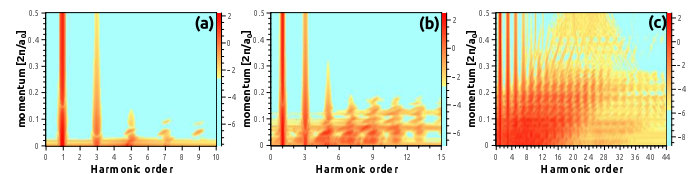


FIG. 3. Fourier transform of the velocity distribution of electrons along the Λ line in the Brillouin zone. The peak laser intensity is: (a) $I=2$ TW/cm², (b) $I=10$ TW/cm² and (c) $I=30$ TW/cm²

- 1 J. Isberg, J. Hammersberg, E. Johansson, T. Wikström, D. J. Twitchen, A. J. Whitehead, S. E. Coe, and G. A. Scarsbrook, *Science* **297**, 1670 (2002).
- 2 A. McPherson, G. Gibson, H. Jara, U. Johann, T. S. Luk, I. A. McIntyre, K. Boyer, and C. K. Rhodes, *J. Opt. Soc. of Am. B* **4**, 595-601 (1987).
- 3 M. Ferray, A. L'Huillier, X. F. Li, L. A. Lompre, G. Mainfray and C. Manus, *J. Phys. B: At. Mol. Opt. Phys.* **21** L31, (1988).
- 4 K. C. Kulander, K. J. Schafer, J. L. Krause, *Super-Intense Laser-Atom Physics*. Ed. B. Piraux, A. L'Huillier, and K. Rzazewski. D. Reidel Publishing Company, Dordrecht-Holland. NATO Advanced Study Institutes Series. B **316**, 95 (1993).
- 5 A. L'Huillier and P. Balcou, *Phys. Rev. Lett.* **70**, 774 (1993)
- 6 J. J. Macklin, J. D. Kmetec, and C. L. Gordon, *Phys. Rev. Lett.* **70**, 766 (1993)
- 7 I. P. Christov, M. M. Murnane, and H. C. Kapteyn, *Phys. Rev. Lett.* **78**, 1251 (1997)
- 8 U. Teubner and P. Gibbon, *Rev. Mod. Phys.* **81**, 445 (2009)
- 9 S. Ghimire et al, *Nature Physics* **3**, 381 (2011).
- 10 M. Abd-Elmeguid et al., *Tesla Technical Design Report, The X-ray Free Electron Laser (DESY, Hamburg, 2001)*
- 11 H. Winick Ed., *Synchrotron Radiation Sources*, World Scientific Pub. Co. Inc., World Scientific Series on Synchrotron Radiation Techniques(1995).

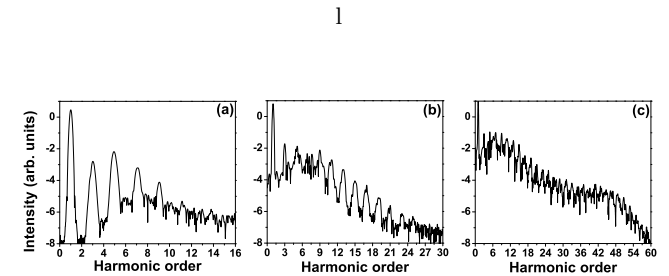


FIG. 4. HHG spectra obtained for photon energy 1.55 eV and pulse duration 15 fs. The peak laser intensity is 2,10 and 30 TW/cm²

- 12 G. Farkas and C. Toth, *Phys. Lett. A* **168**, 447 (1992)
- 13 P. B. Corkum and F. Krausz, *Attosecond Science*, *Nat. Phys.*, **3**, 381, (2007)
- 14 F. Krausz and M. Ivanov, *Rev. Mod. Phys.* **81**, 163 (2009)
- 15 I. P. Christov, M. M. Murnane, and H. C. Kapteyn, *Optics Communications*, **148**, 75 (1998)
- 16 M. Schultze, K. Ramasesha, C.D. Pemmaraju, S.A. Sato, D. Whitmore, A. Gandman, James S. Prell, L. J. Borja, D. Prendergast, K. Yabana, D. M. Neumark, S. R. Leone, *Science* **12 Dec 2014**: Vol. 346, Issue 6215, pp. 1348-1352, DOI: 10.1126/science.1260311

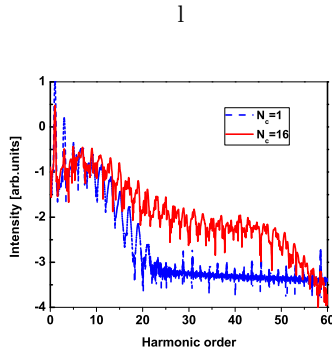


FIG. 5. HHG spectra in diamond bulk obtained for photon energy 1.55 eV, pulse duration 15 fs and peak intensity 30 TW/cm². The number of conduction bands is $N_c = 1$ (dashed curve) and $N_c = 16$ (solid curve)

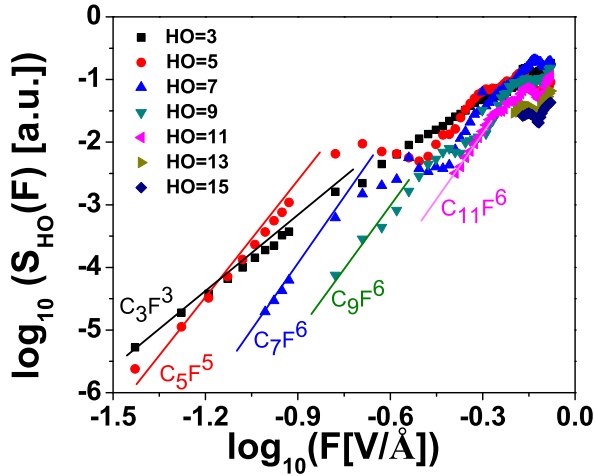


FIG. 6. Dependence of the spectral intensity of individual harmonics on the electric field strength for 15fs laser pulse with photon energy 1.55 eV interacting with bulk diamond

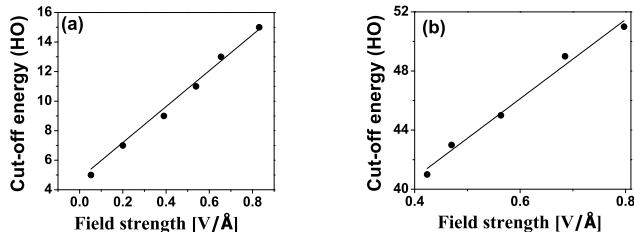


FIG. 7. High-energy cutoff as a function of the driving laser field for the primary plateau in Fig.(a) and the secondary plateau in Fig.(b)

- 17 N. H. Chapman, P. Fromme, A. Barty et al, Femtosecond X-ray protein nanocrystallography, *Nature* 470, 73, 2011
- 18 M. Lewenstein, Ph. Balcou, M. Yu. Ivanov, A. L'Huillier, and P. B. Corkum, *Phys. Rev. A* 49, 2117 (1994)
- 19 P. B. Corkum, *Phys. Rev. Lett.* **71**, 1994 (1993).
- 20 K. J. Schafer, Baorui Yang, L. F. DiMauro, and K. C. Kulander, *Phys. Rev. Lett.* **70**, 1599 (1993).
- 21 G. Ndabashimiye, S. Ghimire, M. Wu, D. A. Browne, K. J. Schafer, M. B. Gaarde and D. A. Reis, *Nature* **522**, 462 (2016), doi:10.1038/nature17660
- 22 T. T. Luu, M. Garg, S. Y. Kruchinin, A. Moulet, M. T. Hassan, and E. Goulielmakis, *Nature (London)* 521, 498 (2015)
- 23 T. Otobe, *Journal of Applied Physics* 111, 093112 (2012), T. Otobe, K. Yabana, and J.-I. Iwata, *Journal of Computational and Theoretical Nanoscience*, 6, 2545, 2009
- 24 T. Otobe, *Journal of Applied Physics* 111, 093112 (2012)
- 25 T. Otobe, *PHYSICAL REVIEW B* 94, 235152 (2016)
- 26 N. Tancogne-Dejean, O. D. Mucke, F. X. Kartner, and A. Rubio, *PRL* 118, 087403 (2017)
- 27 T. Higuchi, M. I. Stockman, and P. Hommelhoff, *Phys. Rev. Lett.* **113**, 213901, (2014).
- 28 M. Wu, S. Ghimire, D. A. Reis, K. J. Schafer, and M. B. Gaarde, *Phys. Rev. A* **91**, 043839, (2015).
- 29 O. Schubert, M.Hohenleutner, F. Langer, B. Urbanek, C. Lange, U. Huttner, D. Golde, T. Meier, M. Kira, S. W. Koch, and R. Huber, *Nat. Photonics* 8, 119 (2014).
- 30 T. T. Luu and H. J. Weorner *Phys. Rev. B* 94, 115164 (2016)
- 31 G. Vampa, C. R. McDonald, G. Orlando, P. B. Corkum, and T. Brabec, *Phys. Rev. B* **91**, 064302 (2015)
- 32 S. Lagomarsino, S. Sciortino, B. Obreshkov, T. Apostolova, C. Corsi, M. Bellini, E. Berdermann, and C. J. Schmidt, *Phys. Rev. B* **93**, 085128, (2016).
- 33 L. V. Keldysh, *Sov. Phys. JETP* 20, 1307 (1965).